SI Materials and Methods

Cloning. *Aae* σ^N or $\Delta N\sigma^N$ (Aae σ^N residues 61-398) were amplified from *Aae* genomic DNA (gift of K.O. Stetter, Uniersity of Regensburg, Germany) by PCR using primers introducing *Nde*I and *Bam*HI sites upstream and downstream of the fragment, respectively, and cloned into a pET28A (Novagen) derivative containing a Precission protease-cleavable His_{10}-tag immediately upstream of the *Nde*I site. The derived plasmid was subjected to site-directed mutagenesis (Stratagene Quikchange) to obtain $\Delta N\sigma^N$ mutants H304A, E305A, E305Q, E305S, S306A, T307A, S309A, and R310A.

Protein expression and purification. *Eco* BL21-CodonPlus (DE3)-RIL cells (Agilent Technologies) were transformed with the approprite expression plasmid containing *Aae* σ^N, $\Delta N\sigma^N$ or $\Delta N\sigma^N$ variants and cells were grown in the presence of 35 μg/mL chloramphenicol and 50 μg/mL kanamycin at 37^{o}C to an OD_{600} of 0.6, whereupon protein expression was induced with 0.5 mM (final concentration) isopropyl-β-D-thiogalactopyranoside (IPTG) for 3 hours. Cells were harvested by centrifugation and resuspended in lysis buffer [20 mM Tris-HCl, pH 8.0, 0.5 M NaCl, 1 mM β-mercaptoethanol, 5% (v/v) glycerol] supplemented with
1 mM phenylmethylsulfonyl fluoride and protease inhibitor cocktail (Sigma-Aldrich). Cells were then lysed by a continuous-flow French press (Avestin) and the lysate was cleared by centrifugation. The clarified lysate was heat-treated at 65 ^{o}C for 40 minutes and re-centrifuged. The desired *Aae* protein in the soluble fraction was subsequently loaded onto a Hi-Trap IMAC Ni^{2+}-Chelating Column (GE Healthcare) and eluted with

lysis buffer + 250 mM imidazole. PreScission Protease (GE Healthcare) was added to the eluted protein to cleave the His_{10}-tag and the sample was dialyzed into lysis buffer + 12.5 mM imidazole and re-loaded onto the Hi-Trap IMAC Ni^{2+}-Chelating Column to purify the cleaved protein, which eluted in the flow-through. The protein was precipitated by adding ammonium sulfate to 2.7 M and the precipitate was pelleted by centrifugation and then resuspended in 20 mM Tris-HCl, pH 8.0, 0.5 M NaCl, 5 mM DTT, 5% (v/v) glycerol and loaded on a size exclusion column (HiLoad 16/600 Superdex 200; GE Healthcare). The protein was ammonium sulfate precipitated as before and stored in aliquots at -80 ^{o}C. The $\Delta N\sigma^{N}$ variants E305Q and E305S were poorly soluble when expressed at 37^{o}C so their expression was induced with 0.1 mM IPTG for 16 hours at 16 ^{o}C. Cells were harvested, lysed, and the proteins were purified as above.

Radioactive Filter Binding Assay. The *dhsU* promoter DNA and mutant derivatives (Tables 1, 2) were prepared by radio-labeling the 5' end of one oligonucleotide using [γ^{32}P]ATP and purifying the strand using a Sepharose G-50 column (GE Healthcare), followed by annealing the labeled strand with a 1.5-fold molar excess of unlabeled complementary oligonucleotide. Reactions (40 µL) were set up with 0.625 nM DNA and varying concentrations (0, 1, 3, 10, 30, 100, 300, 1000, and 3000 nM) of full-length σ^{N}, $\Delta N\sigma^{N}$ or $\Delta N\sigma^{N}$ mutants (Table 2) in binding buffer (10 mM Tris-HCl, pH 8.0, 250 mM NaCl) at 25^{o}C for 30 minutes. Sterilized 0.45 µm nitrocellulose filters (Millipore) were placed in a vacuum filter-binding assay apparatus (Millipore) and pre-washed with binding buffer. Reaction mixtures (35 µL) were then pipetted onto the filter and washed

with 5 mL binding buffer. Filters were air-dried and visualized by phosphorimagery. Filter-bound complexes were quantified using ImageQuant 5.2.

Crystallization of the *Aae* ΔNσ^N/DNA complex. To prepare the DNA, lyophilized oligonucleotides (Oligos Etc.) were dissolved in 20 mM Tris-HCl, pH 8.0, 0.5 mM EDTA, 0.2 M NaCl to a concentration of 2 mM. Equimolar amounts of the complementary oligonucleotides were annealed by heating to 95^{o}C for 5 min followed by slow cooling to 25 ^{o}C, to obtain 1 mM duplex promoter.

Ammonium sulfate precipitated *Aae* ΔNσ^N was pelleted by centrifugation and resolubilized in crystallization buffer (10 mM Tris-HCl, pH 8.0, 0.2 M NaCl, 5 mM DTT). The ΔNσ^N-promoter complex was formed by adding promoter DNA to protein (1.2:1 molar ratio) and incubating for 10 minutes at 4^{o}C. The complex was buffer exchanged into crystallization buffer and concentrated to a final protein concentration of 10 mg/mL by centrifugal filtration (VivaScience). Crystals of the ΔNσ^N-promoter complex were obtained by sitting drop vapor diffusion at 22 ^{o}C by mixing 1 uL of sample with 1 uL of reservoir solution (50 mM sodium cacodylate, pH 6.5, 0.2 M KCl, 0.1 M Mg-acetate, 14%-18% Polyethylene glycol 8000). Crystals appeared after 3 days, sometimes growing quite large (~500 μm in dimensions). The crystals were transferred into reservoir solution supplemented with 20% (v/v) glycerol for cryoprotection and flash frozen in liquid nitrogen.

Data collection, structure determination, and refinement of the *Aae* $\Delta N\sigma^N$/DNA complex. X-ray diffraction data were collected at the Argonne National Laboratory Advanced Photon Source NE-CAT beamline 24-ID-C and Brookhaven National Laboratory National Synchrotron Light Source beamiline X3A. Most structural biology software was accessed through the SBGrid consortium (1). Data were integrated and scaled using HKL2000 (2). The crystals belonged to space group $P3_2$ (Table S1) but analysis using XTRIAGE within PHENIX (3) revealed that the crystals were often twinned (operator *h*, *-h-k*, *-l*), with variable twinning fraction. A large number of crystals were screened to find the best diffracting datasets that were also not twinned. Two datasets were combined for the final native dataset used in refinement (Table S1).

Phasing proved to be problematic. Crystals containing selenomethionyl-substituted $\Delta N\sigma^N$ were produced but these diffracted poorly and did not yield useful anomalous information, possibly because of nonisomorphism. Many heavy atom soaks were attempted but these either did not bind to the crystals or destroyed the diffraction if they did. Useful phasing information was obtained using Ta_6Br_{14} (4). Ta_6Br_{14} (Jena Bioscience) was added directly to hanging drops containing crystals (final concentration ~1 mM). Over a soaking time of ~1 hr the crystals turned greenish blue and were cryoprotected (effectively back-soaking as well) and flash frozen as for the native crystals. X-ray data for Ta_6Br_{14}-soaked crystals was collected at NSLS beamline X3A at a wavelength of 1.2568 Å (Ta L-edge). SHELX (5) identified four Ta sites, and a fifth was identified subsequently by difference Fourier methods. Phasing was performed with SHARP/autoSHARP (6), incorporating both the anomalous signal from the Ta-

cluster and isomorphous differences between the Ta_6Br_{14}-soaked crystals and the native crystals.

The initial electron density map was poor but contained recognizable features for duplex DNA as well as some protein α-helices (such as the -12BD-ELH). Generic B-form duplex DNA and poly-Ala α-helices were fit into the map and refined as rigid bodies using PHENIX (3). Phase combination yielded an improved electron density map that allowed the placement of the CBD (PDB ID 2KM9) (7) and the RpoN domain bound to -24 element DNA (PDB ID 2O9L)(8). The latter fit fixed the register of the DNA, allowing the modeling of the rest of the DNA sequence. The model was improved by iterative cycles of manual building with COOT (9), and refinement with PHENIX (3) using 2-fold non-crystallographic symmetry restraints.

Re-building and re-refinement of $E\sigma^N$ using the deposited structure factors associated with 5BYH. As a starting model, we used coordinates of *Eco* core RNAP derived from *Eco* $\Delta 1.1\sigma^{70}$-holoenzyme with $\Delta 1.1\sigma^{70}$ removed (PDB ID 4LJZ)(10) superimposed onto the *Eco* core RNAP of 5BYH (11) using the 'align' command in PyMOL (The PyMOL Molecular Graphics System, Version 1.6 Schrödinger, LLC). Using PHENIX (3), an initial rigid body refinement was done with the entire core RNAP molecule as one rigid body (Table S4, step 1), followed by rigid body refinement of 15 individual mobile domains (Table S4, step 2). After this step, strong Fourier difference density attributable to the σ^N domains was evident.

For initial models of the *Kpn* σ^N domains (CBD, -12BD, RpoN domain), we generated homology models using the *Aae* σ^N domains as templates using the Swiss Model Server (12). These domains were manually fit into the difference density and a further round of rigid body refinement was performed that included the three σ^N domains. We then subjected the structure to a round of deformable elastic network refinement using CNS 1.3 performed on the Structural Biology Grid cluster (13-15), followed by an all atom PHENIX refinement (Table S4, step 3). The model was subsequently improved by iterative rounds of manual building (COOT) (9) and refinement with PHENIX (Table S3, Table S4, step 4).

Yang et al. (11) collected data from Eσ^N crystals containing selenomethionyl-substituted *Kpn* σ^N and used the calculated anomalous Fourier difference peaks to locate 8 out of 11 possible methionines (Fig. S1A of (11)), so the large corrections required in our model of Eσ^N (Fig. S5) were surprising. However, 7 of the 8 methionine positions identified were in regions of the σ^N structure that had a registration error of 0 or 1 (Table S5), and the distances between the methionine Sε atoms in 5BYH and our corrected Eσ^N model were within the error of the size of the anomalous difference peaks (equal to or less than 3.7 Å; Table S5). Only one position (M306) was in a region of the structure with a large registration error of 5, and the methionine Sε atom displacement between the two models was large (13.8 Å; Table S5). However, close examination of Fig. S1A of (11) reveals that M306 in 5BYH does not appear to overlap with the anomalous difference peak, possibly explaining the discrepancy.

Supplemental references

1. Morin A, et al. (2013) Collaboration gets the most out of software. *Elife* 2:e01456.

2. Otwinowski Z, Minor W (1997) Processing of X-ray diffraction data collected in oscillation mode. *Methods Enzymol* 267:307–326.

3. Adams PD, et al. (2010) PHENIX: a comprehensive Python-based system for macromolecular structure solution. *Acta Crystallogr D Biol Crystallogr* 66(Pt 2):213–221.

4. Knäblein J, et al. (1997) Ta6Br(2+)12, a tool for phase determination of large biological assemblies by X-ray crystallography. *J Mol Biol* 270(1):1–7.

5. Sheldrick GM (2008) A short history of SHELX. *Acta Crystallogr, A, Found Crystallogr* 64(Pt 1):112–122.

6. Vonrhein C, Blanc E, Roversi P, Bricogne G (2007) Automated structure solution with autoSHARP. *Methods Mol Biol* 364:215–230.

7. Hong E, Doucleff M, Wemmer DE (2009) Structure of the RNA Polymerase Core-Binding Domain of σ54 Reveals a Likely Conformational Fracture Point. *J Mol Biol* 390(1):70–82.

8. Doucleff M, Pelton JG, Lee PS, Nixon BT, Wemmer DE (2007) Structural Basis of DNA Recognition by the Alternative Sigma-factor, σ54. *J Mol Biol* 369(4):1070–1078.

9. Emsley P, Cowtan K (2004) Coot: model-building tools for molecular graphics. *Acta Crystallogr D Biol Crystallogr* 60(Pt 12 Pt 1):2126–2132.

10. Bae B, et al. (2013) Phage T7 Gp2 inhibition of Escherichia coli RNA polymerase involves misappropriation of σ70 domain 1.1. *Proc Natl Acad Sci USA* 110(49):19772–19777.

11. Yang Y, et al. (2015) TRANSCRIPTION. Structures of the RNA polymerase-σ54 reveal new and conserved regulatory strategies. *Science* 349(6250):882–885.

12. Arnold K, Bordoli L, Kopp J, Schwede T (2006) The SWISS-MODEL workspace: a web-based environment for protein structure homology modelling. *Bioinformatics* 22(2):195–201.

13. Schröder GF, Levitt M, Brunger AT (2010) Super-resolution biomolecular crystallography with low-resolution data. *Nature* 464(7292):1218–1222.

14. Brunger AT, Adams PD, Clore GM (1998) Crystallography & NMR system: a new software suite for macromolecular structure determination. *Acta Crystallogr D Biol Crystallogr* 54:905–921.

15. O'Donovan DJ, et al. (2012) A grid-enabled web service for low-resolution crystal structure refinement. *Acta Crystallogr D Biol Crystallogr* 68(Pt 3):261–267.

16. Karplus PA, Diederichs K (2012) Linking Crystallographic Model and Data Quality. *Science* 336(6084):1030–1033.

17. Doucleff M, Malak LT, Pelton JG, Wemmer DE (2005) The C-terminal RpoN domain of sigma54 forms an unpredicted helix-turn-helix motif similar to domains of sigma70. *J Biol Chem* 280(50):41530–41536.

18. Studholme DJ, Wigneshwereraraj SR, Gallegos MT, Buck M (2000) Functionality of purified sigma(N) (sigma(54)) and a NifA-like protein from the hyperthermophile Aquifex aeolicus. *J Bact* 182(6):1616–1623.

19. Barrios H, Valderrama B, Morett E (1999) Compilation and analysis of sigma(54)-dependent promoter sequences. *Nucl Acids Res* 27(22):4305–4313.

20. Stivala A, Wybrow M, Wirth A, Whisstock JC, Stuckey PJ (2011) Automatic generation of protein structure cartoons with Pro-origami. *Bioinformatics* 27(23):3315–3316.

Table S1. Crystallographic statistics for $\Delta N\sigma^N$/DNA crystals

Data collection	Native	Ta_6Br_{14}
Space group	$P3_2$	$P3_2$
Combined datasets	2	1
Cell dimensions		
a, b, c (Å)	99.92, 99.92, 123.3	99.92, 99.92, 120.8
α, β, γ (°)	90, 90, 120	90, 90, 120
Resolution (Å)	15 – 3.4 (3.52 – 3.4)[a]	35 – 5.80 (6.01 – 5.80)
Total reflections	246,017 (14,226)	20,719 (1,299)
Unique reflections	18,717 (1,882)	7,301 (649)
Multiplicity	13.1 (7.5)	2.8 (2.0)
Completeness (%)	99 (100)	97.1 (87.2)
$\langle I \rangle / \sigma I$	20.42 (2.37)	25.4 (2.57)
Wilson B-factor	119.74	
R_{pim}[b]	0.040 (0.340)	
CC1/2[b]	0.999 (0.556)	
CC*[b]	1.0 (0.845)	
Refinement		
R_{work} / R_{free}	0.2887/0.3356 (0.3949/0.4414)	
CC_{work}/CC_{free}[c]	0.956/0.939 (0.490/0.227)	
No. non-hydrogen atoms	7,788	
Protein	5,258	
DNA	2,498	
Water	32	
Protein residues	639	
B-factors		
Protein	120.5	
DNA	159.3	
Water	91.14	
R.m.s deviations		
Bond lengths (Å)	0.004	
Bond angles (°)	0.91	
Clashscore	39.39	
Ramachandran favored (%)	96	
Ramachandran outliers (%)	0.16	

[a] Values in parentheses are for highest-resolution shell.

[b] As calculated by HKL2000.

[c] (16).

Table S2. Results of σ^N domain superpositions.

Superimposition of A -> B[a]	Rmsd (Å)[a]	# of α carbons[a]
B: *Aae* CBDa(molA)		
A: *Aae* CBDa(molB)	0.642	67
A: *Aae* CBDa (2KM9)[b]	1.494	64
A: *Kpn* CBDa (5BYH)[c]	2.417	49
B: *Aae* CBDb(molA)		
A: *Aae* CBDb(molB)	0.521	47
A: *Aae* CBDb (2KM9)[b]	1.296	44
A: *Kpn* CBDb (5BYH)[c]	5.79	36
B: *Aae* -12BD(molA)		
A: *Aae* -12BD(molB)	0.422	116
A: *Kpn* -12BD (5BYH)[c]	8.372	103
B: *Aae* RpoN domain(molA)		
A: *Aae* RpoN domain(molB)	0.599	48
A: *Aae* RpoN domain (2AHQ)[d]	1.234	40
A: *Aae* RpoN domain (2O8K)[e]	1.303	50
A: *Aae* RpoN domain (2O9L)[e]	1.051	48
A: *Kpn* RpoN domain (5BYH)[c]	0.792	40

[a] Superimpositions performed using the PyMOL 'align' command (The PyMOL Molecular Graphics System, Version 1.6 Schrödinger, LLC).

[b] (7).

[c] (11).

[d] (17).

[e] (8).

Table S3. Eσ^N Crystallographic statistics.

	5BYH[a]	5BYH[b]	5BYH[c]	Corrected 5BYH
Data collection				
Space group	$P2_12_12$			
Cell dimensions				
a, b, c (Å)	208.48, 151.52, 195.28			
α, β, γ (°)	90, 90, 90			
Resolution (Å)	29.8 – 3.76 (3.89 – 3.76)[d]			
Multiplicity	8.3 (4.7)			
Completeness (%)	98.4 (91.2)			
$\langle I \rangle / \sigma I$	14.1 (1.9)			
Wilson B-factor	119.19			
R_{pim}	0.042 (0.45)			
CC1/2	0.999 (0.845)			
Refinement				
No. reflections	62,409		62,365	62,373
No. test reflections	3,077		3,074	3,074
R_{work} / R_{free}[e]	0.3313/0.3402	0.347/0.353	0.342/0.378	0.262/0.312
CC_{work}/CC_{free}			0.744/0.658	0.855/0.782
Error estimates (maximum-likelihood based)[f]				
Coordinate error (Å)			0.68	0.52
Phase error			46.01°	37.67°
No. non-hydrogen atoms				
Protein	22,647	22,891	22,897	27,002
Ligand/ion	1		3	3
Average B-factors (Å^2)	200.9	209.8	194.08	173.4
R.m.s deviations				
Bond lengths (Å)	0.007		0.004	0.003
Bond angles (°)	0.99	1.03	0.903	0.775
Clashscore	0.3		1.91	15.58
Ramachandran favored (%)	85.5		87.98	90.6
Ramachandran allowed (%)	11.3		9.73	9.06
Ramachandran outliers (%)	3.2		2.29	0.04

[a] As reported in (11), Table S1

[b] Reported in 5BYH PDB file header (when different from (11), Table S1)

[c] 5BYH refined using PHENIX (identical settings as for the corrected 5BYH).

[d] Values in parentheses are for highest-resolution shell.

[e] The same R_{free} test set was used throughout.

[f] As reported in PDB file header by PHENIX (3).

Table S4. Progress of 5BYH re-refinement.

Step[a]	R_{work}	R_{free}	CC_{work}	CC_{free}	bonds	angles	Ramachandran outliers (%)	MolProbity score
1. Rigid body refinement starting with 4LJZ	0.468	0.468	0.468	0.439				
2. Rigid body refinement (domains)	0.423	0.418	0.574	0.567				
3. All atom refinement after DEN refinement	0.354	0.403	0.697	0.602	0.005	0.854	0.7	3.18
4. Final refinement	0.264	0.313	0.851	0.773	0.004	0.860	0.44	3.16

[a] All refinements and statistics as reported by PHENIX (3).

Table S5. Methionine Sε atom displacements between 5BYH and our corrected Eσ^N model.

Kpn σ^N methionine position	Registration error between new Eσ^N model and 5BYH	Distance between Met Sε atoms (Å)
125	0	0.7
236	-1	2.6
306	5	13.8
362	1	3.7
365	1	1.2
376	0	0.8
445	0	0.7
452	0	1.4

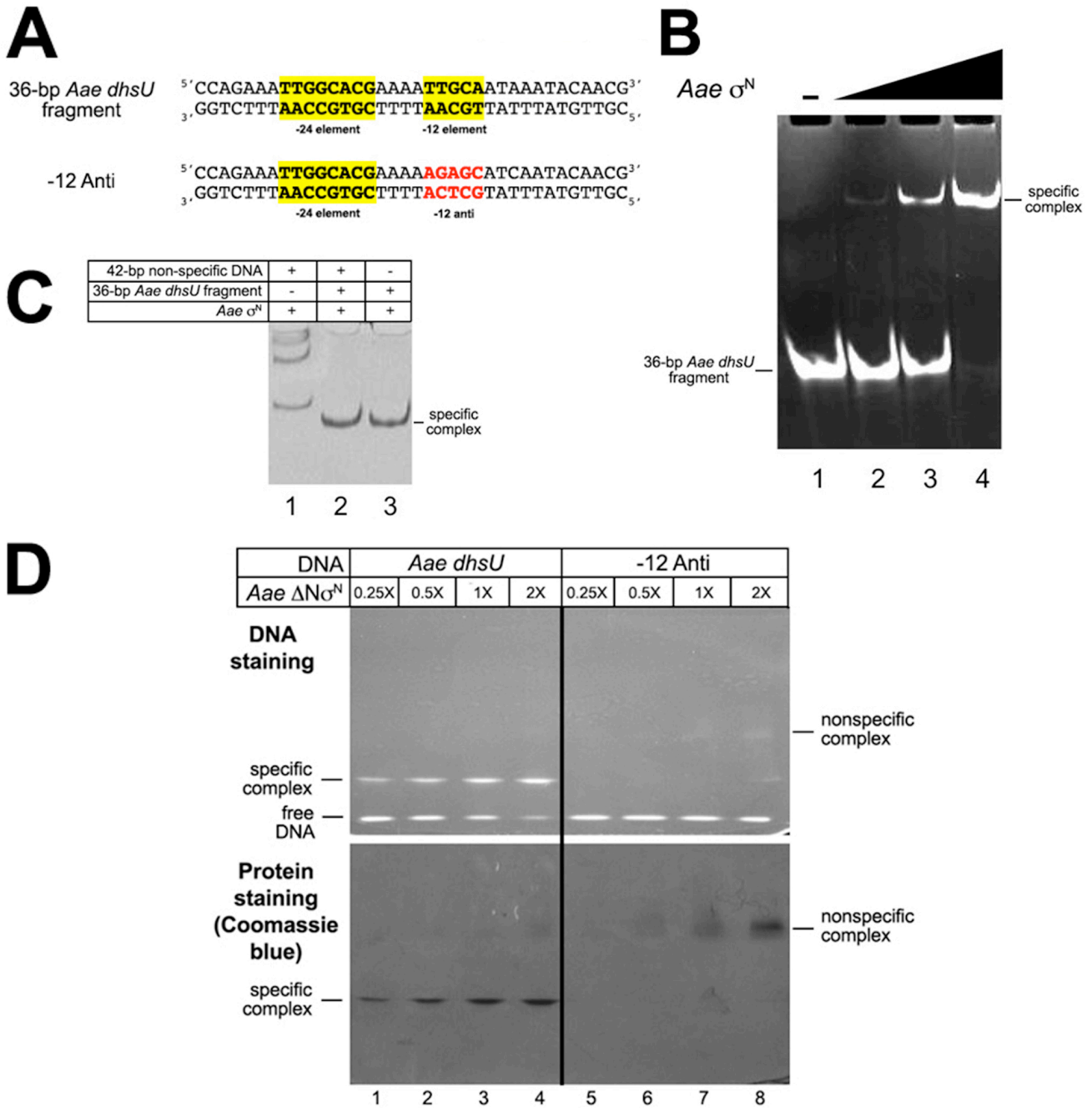
A
36-bp Aae dhsU fragment
5′CCAGAAATTGGCACGAAAATTGCAATAAATACAACG3′
3′GGTCTTTAACCGTGCTTTTAACGTTATTTATGTTGC5′
-24 element
-12 element
-12 Anti
5′CCAGAAATTGGCACGAAAAAGAGCATCAATACAACG3′
3′GGTCTTTAACCGTGCTTTTACTCGTATTTATGTTGC5′
-24 element
-12 anti
B
Aae σN
specific complex
36-bp Aae dhsU fragment
1 2 3 4
C
42-bp non-specific DNA + + -
36-bp Aae dhsU fragment - + +
Aae σN + + +
specific complex
1 2 3
D
DNA
Aae dhsU
-12 Anti
Aae ΔNσN
0.25X 0.5X 1X 2X 0.25X 0.5X 1X 2X
DNA staining
nonspecific complex
specific complex
free DNA
Protein staining (Coomassie blue)
nonspecific complex
specific complex
1 2 3 4 5 6 7 8

Figure S1

Figure S1. Specific DNA binding by *Aae* σ^N and $\Delta N\sigma^N$.

(**A**) Sequences of (top) *Aae dhsU* promoter fragment (18) and -12 anti promoter fragment, containing the least likely base to occur at each position of the -12 element (19).

(**B**) Native gel electrophoresis showing discrete complex formation between *Aae* σ^N and the 36-bp *dhsU* promoter fragment. The gel is visualized with GelRed (Biotium).

(**C**) Native gel electrophoresis showing specific complex formation between *Aae* σ^N and the 36-bp *dhsU* promoter fragment by challenging with a 100-fold molar excess of a non-specific DNA sequence. The gel is visualized with Coomassie blue.

(**D**) Native gel electrophoresis showing specific complex formation between *Aae* $\Delta N\sigma^N$ and the 36-bp *dhsU* promoter fragment (left panels), compared to non-specific complexes on the -12 anti fragment (right panels). The top and bottom panels are the same gel, only the top is visualized with GelRed, while the bottom is visualized with Coomassie blue.

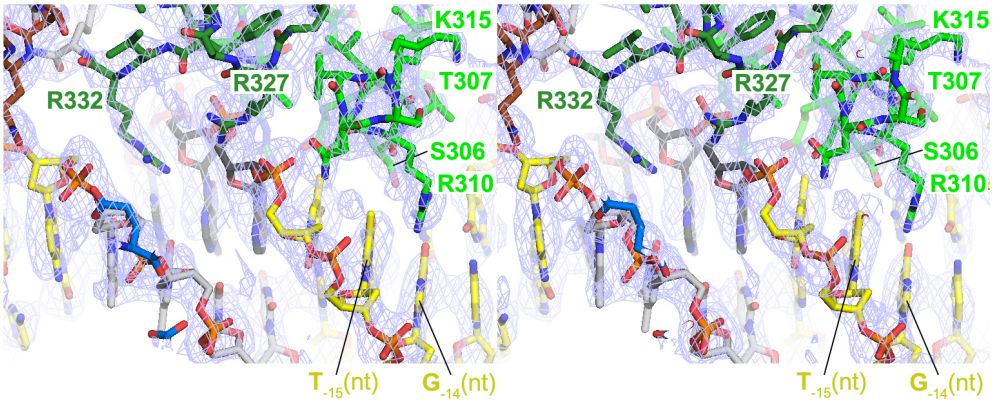
K315
R332
R327
T307
S306
R310
T-15(nt)
G-14(nt)
K315
R332
R327
T307
S306
R310
T-15(nt)
G-14(nt)

Figure S2

Figure S2. Electron density for *Aae* $\Delta N\sigma^N$/DNA.

Stereo view of the final $2F_o - F_c$ electron density map from the *Aae* $\Delta N\sigma^N$/DNA structure, contoured at 1.2σ. The final model is superimposed.

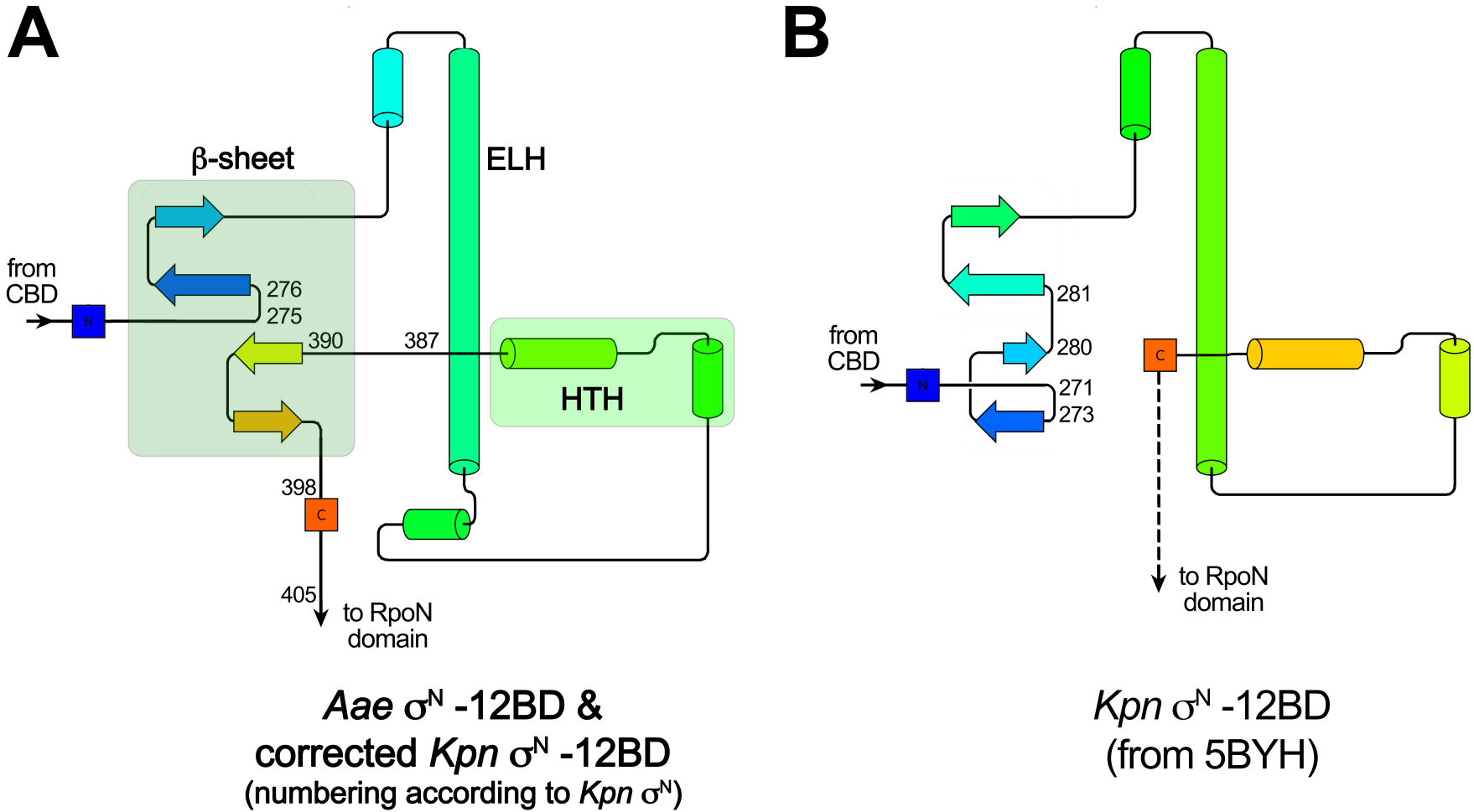

Aae σ^N -12BD &
corrected *Kpn* σ^N -12BD
(numbering according to *Kpn* σ^N)

Kpn σ^N -12BD
(from 5BYH)

Figure S3

Figure S3. Secondary structure topology diagrams for the -12BD.

(**A**) Secondary structure topology diagram of the *Aae* σ^N -12BD and the corrected *Kpn* σ^N. The secondary structure elements are colored in a ramp from the N-terminus (blue) to the C-terminus (red) of the -12BD. The amino acid numbering is according to the *Kpn* σ^N sequence and mark segments of the structure absent in the original *Kpn* σ^N from 5BYH (11).

(**B**) Secondary structure topology diagram of the *Kpn* σ^N from 5BYH (11). The secondary structure elements are colored in a ramp from the N-terminus (blue) to the C-terminus (red) of the -12BD. The amino acid numbering marks incorrect connections.

The secondary structure topology diagrams were made with the assistance of Pro-Origami (20).

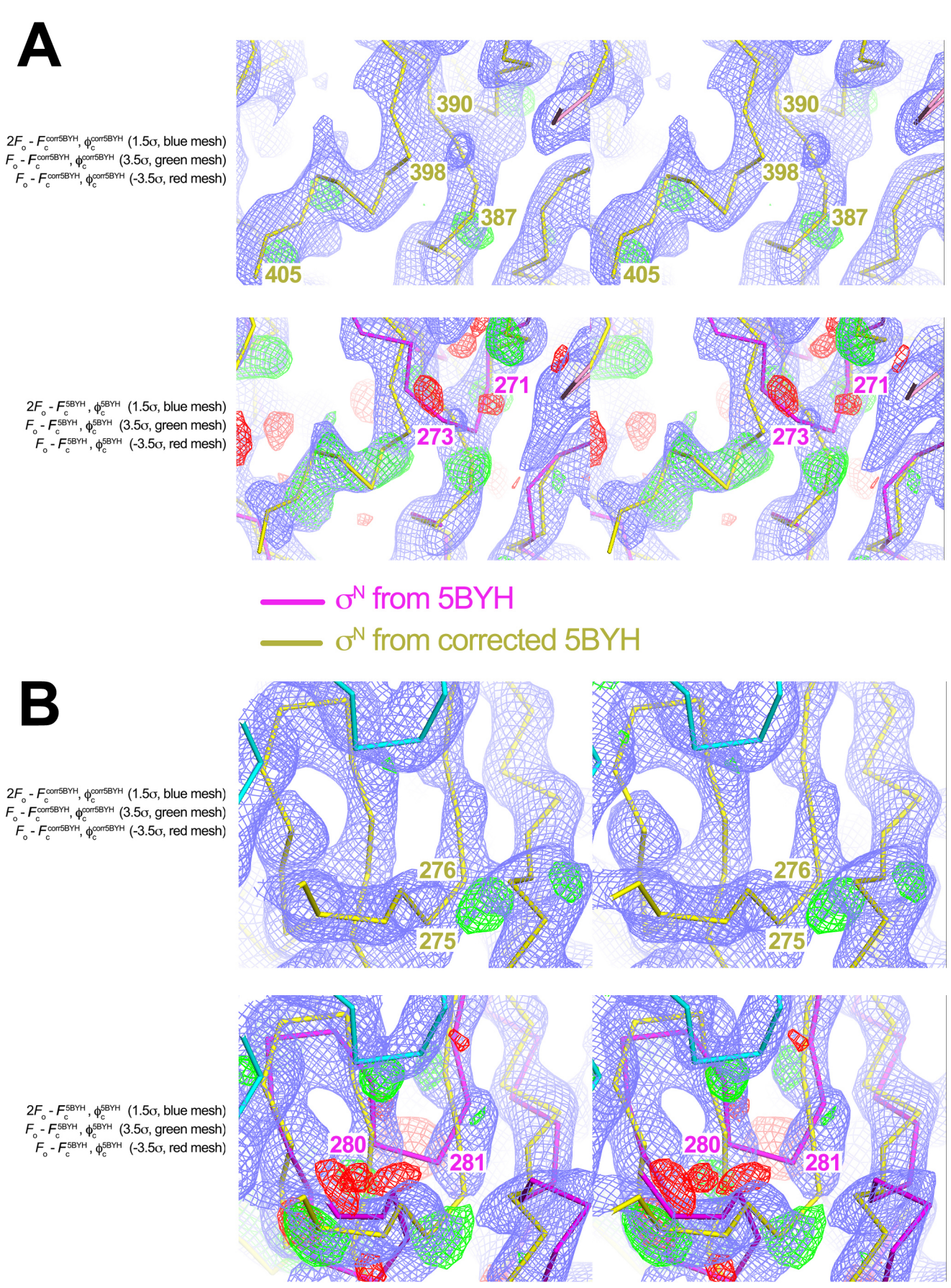
A
$2F_o - F_c^{corr5BYH}, \phi_c^{corr5BYH}$ (1.5σ, blue mesh)
$F_o - F_c^{corr5BYH}, \phi_c^{corr5BYH}$ (3.5σ, green mesh)
$F_o - F_c^{corr5BYH}, \phi_c^{corr5BYH}$ (-3.5σ, red mesh)
390
398
387
405
$2F_o - F_c^{5BYH}, \phi_c^{5BYH}$ (1.5σ, blue mesh)
$F_o - F_c^{5BYH}, \phi_c^{5BYH}$ (3.5σ, green mesh)
$F_o - F_c^{5BYH}, \phi_c^{5BYH}$ (-3.5σ, red mesh)
271
273
σ^N from 5BYH
σ^N from corrected 5BYH
B
$2F_o - F_c^{corr5BYH}, \phi_c^{corr5BYH}$ (1.5σ, blue mesh)
$F_o - F_c^{corr5BYH}, \phi_c^{corr5BYH}$ (3.5σ, green mesh)
$F_o - F_c^{corr5BYH}, \phi_c^{corr5BYH}$ (-3.5σ, red mesh)
276
275
$2F_o - F_c^{5BYH}, \phi_c^{5BYH}$ (1.5σ, blue mesh)
$F_o - F_c^{5BYH}, \phi_c^{5BYH}$ (3.5σ, green mesh)
$F_o - F_c^{5BYH}, \phi_c^{5BYH}$ (-3.5σ, red mesh)
280
281

Figure S4

Figure S4. Eσ^N electron density maps.

Stereo views of Fourier difference maps calculated based on the corrected Eσ^N structure and 5BYH (11).

(**A**) (top) stereo view of Fourier difference maps calculated using calculated amplitudes ($F_c^{corr5BYH}$) and phases ($\phi_c^{corr5BYH}$) from the corrected Eσ^N structure. The corrected σ^N is shown as a yellow backbone ribbon. A segment of the β' subunit is also visible (pink ribbon). Connections in the corrected structure that are missing from 5BYH are shown (387-390 and 398-405, see Fig. S3A).

(bottom) Same view as (top), but with Fourier difference maps calculated using calculated amplitudes (F_c^{5BYH}) and phases (ϕ_c^{5BYH}) from 5BYH. The corrected σ^N is shown in yellow, while σ^N from 5BYH is shown in magenta. Strong positive $F_o - F_c^{5BYH}$ density (green mesh) is present in the segments of the corrected σ^N (yellow ribbon) missing from 5BYH. Negative $F_o - F_c^{5BYH}$ density is seen for the 271-273 connection for 5BYH (magenta), which is an incorrect connection (see Fig. S3B).

(**B**) (top) Same as the top in **A** except a different view showing the 275-276 connection (see Fig. S3A). A segment of the β subunit is visible (cyan ribbon).

(bottom) Same view as (top) but with Fourier difference maps calculated using calculated amplitudes (F_c^{5BYH}) and phases (ϕ_c^{5BYH}) from 5BYH. Strong positive $F_o - F_c^{5BYH}$ density (green mesh) is present in the segment of the corrected σ^N (yellow ribbon) missing from 5BYH. The $2F_o - F_c^{5BYH}$ density (blue mesh) does not support the 280-281 connection for 5BYH (magenta, see Fig. S3B).

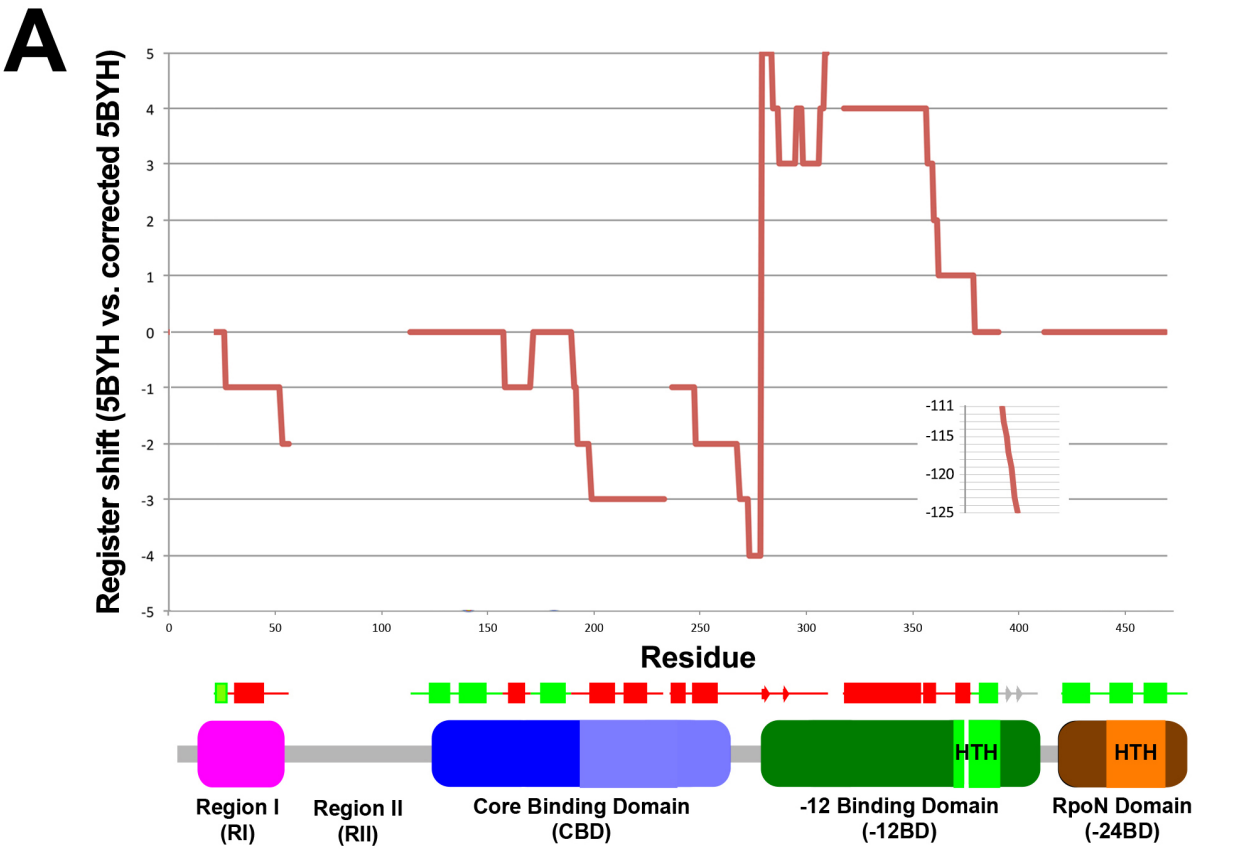
A
Register shift (5BYH vs. corrected 5BYH)
Residue
Region I
(RI)
Region II
(RII)
Core Binding Domain
(CBD)
-12 Binding Domain
(-12BD)
RpoN Domain
(-24BD)
HTH
HTH

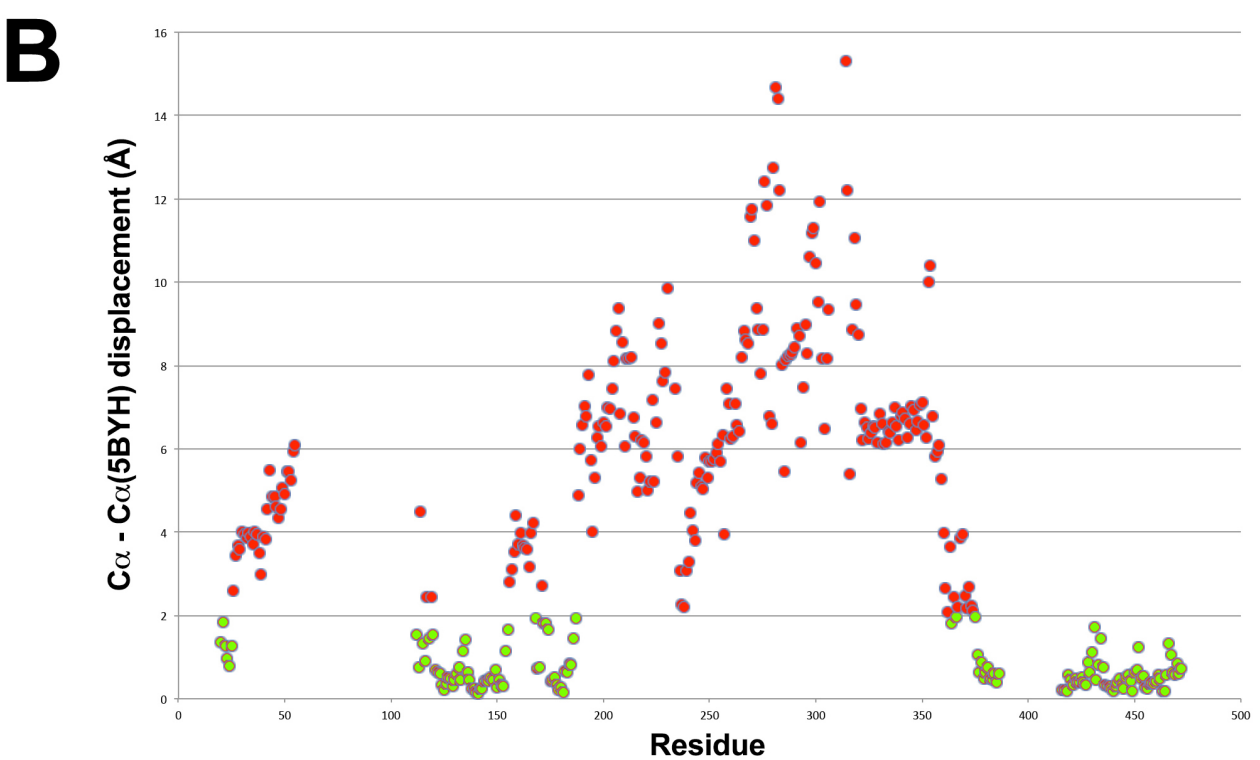
B
Cα - Cα(5BYH) displacement (Å)
Residue

Figure S5

Figure S5. Differences between the *Kpn* σ^N structure of 5BYH and the corrected Eσ^N.

(**A**) Plot showing the register shift in the amino acid sequence of σ^N for 5BYH vs. the corrected 5BYH. Below is shown a schematic of the σ^N domain architecture (colored as in Fig. 1B) and a secondary structure schematic (helices, rectangles; β-strands, arrows). The secondary structure schematic is colored green when the register of σ^N from 5BYH and the corrected 5BYH match, red when it does not match.

(**B**) Plot showing the σ^N $C\alpha^{corr5BYH}$-$C\alpha^{5BYH}$ displacement. Displacements < 2Å were generally in regions of the structure where the sequence register was correct (green dots). Red dots show displacements > 2 Å.

Aae ΔNσ^{N}/DNA

Aae σ^{N}
Kpn σ^{N}

corrected Eσ^{N}

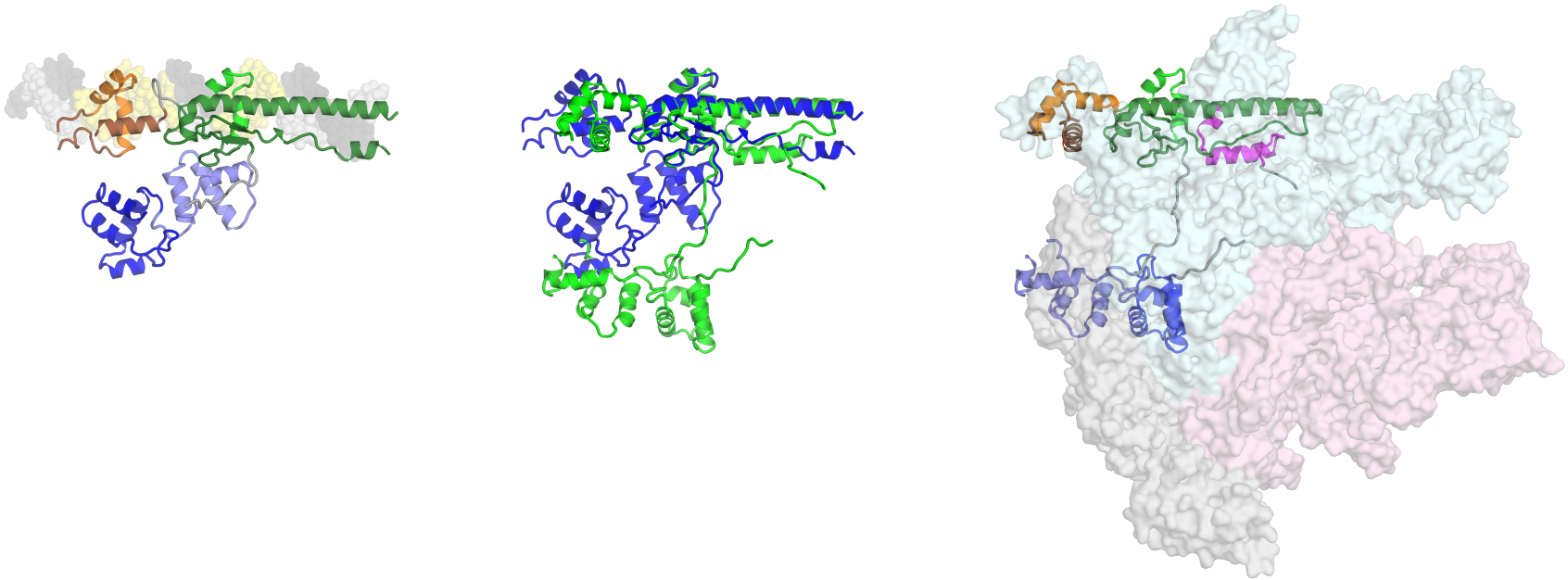

Figure S6

Figure S6. Conformational flexibility of σ^N.

(left) Overall structure of *Aae* $\Delta N\sigma^N$ in the context of the *Aae* $\Delta N\sigma^N$/DNA structure. The *Aae* σ^N is shown as a backbone cartoon and colored according to Fig. 1B.

(right) Overall structure of *Kpn* σ^N in the context of the corrected $E\sigma^N$ structure. The RNAP is shown as a transparent molecular surface (α, ω, grey; β, light cyan; β', light pink). *Kpn* σ^N is shown as a backbone cartoon and colored according to Fig. 1B.

(center) The *Aae* $\Delta N\sigma^N$ (blue) and *Kpn* σ^N (green) are shown together, superimposed by the -12BDs.